Research Article | Vol. 10, No. 4 | 1 Apr 2019 | BIOMEDICAL OPTICS EXPRESS 1891
Biomedical Optics EXPRESS

SyncRGB-FLIM: synchronous fluorescence imaging of red, green and blue dyes enabled by ultra-broadband few-cycle laser excitation and fluorescence lifetime detection

Christian Maibohm,[1] Francisco Silva,[2] Edite Figueiras,[1,4] Paulo T. Guerreiro,[2,3] Marina Brito,[1] Rosa Romero,[2,3] Helder Crespo,[2,3] and Jana B. Nieder[1,*]

[1]*Department of Nanophotonics, Ultrafast Bio- and Nanophotonics Group, INL-International Iberian Nanotechnology Laboratory, Av. Mestre José Veiga n/a, 4715-330 Braga, Portugal*
[2] *Sphere Ultrafast Photonics, R. do Campo Alegre 1021, Edifício FC6, 4169-007 Porto, Portugal*
[3]*IFIMUP-IN and Dept. of Physics and Astronomy, Faculty of Sciences, University Porto, R. do Campo Alegre 697, 4169-007 Porto, Portugal*
[4]*Present address: Fundação Champalimaud, Avenida Brasília, 1400-038 Lisboa, Portugal*
**jana.nieder@inl.int*

Abstract: We demonstrate for the first time that an ultra-broadband 7 femtosecond (fs) few-cycle laser can be used for multicolor nonlinear imaging in a single channel detection geometry, when employing a time-resolved fluorescence detection scheme. On a multi-chromophore-labelled cell sample we show that the few-cycle laser can efficiently excite the multiple chromophores over a >400 nm two-photon absorption range. By combining the few-cycle laser excitation with time-correlated single-photon counting (TCSPC) detection to record two-photon fluorescence lifetime imaging microscopy (FLIM) images, the localization of different chromophores in the cell can be identified based on their fluorescence decay properties. The novel SyncRGB-FLIM multi-color bioimaging technique opens the possibility of real-time protein-protein interaction studies, where its single-scan operation translates into reduced laser exposure of the sample, resulting in more photoprotective conditions for biological specimens.

1. Introduction

Cellular processes govern and are the basis for life, where proteins play a key role. The highly complex cellular mechanics are governed by protein-protein interactions, which allow orchestrated action of chemical processes related to metabolism, cell growth, differentiation, and nutrient uptake, to name a few [1]. Protein-protein interactions often influence chemical reactions in the direct environment and the protein molecular complexes might change their tertiary conformation or intracellular location enabling trafficking, ion/proton transfer or the dislocation of molecules, e.g. along filament strands. These interactions mostly involve multiple constituents and to observe the effect of one protein action in sync with the reacting protein species is not trivial but could potentially enable a deeper understanding of the relevant interactions that govern the basic building blocks of living systems.

Light microscopy in its various forms is still considered a cornerstone and go-to technique accounting for about 80% of the research methodologies used in life sciences. With developments in advanced optical microscopy and through different configurations, light microscopy provides a noninvasive way of imaging the subcellular structure of cells. Contrast between different cellular constituents is created via intensity, lifetime, spectra or labeling [2–6] and optical techniques are therefore perfectly suited to solve the challenge of tracking protein-protein interactions in real time.

#355473 https://doi.org/10.1364/BOE.10.001891
Journal © 2019 Received 3 Jan 2019; revised 1 Feb 2019; accepted 6 Feb 2019; published 18 Mar 2019

Biomedical Optics EXPRESS

Scanning multi-photon microscopy belongs to the family of fluorescence based microscope techniques and has become an integral part of bioimaging where the intrinsic confinement of the excitation light in both the spatial and phase domains enables separation of subcellular features against the neighboring background [5].

Ultrashort pulse lasers are commonly used to generate the necessary photon density for multi-photon microscopy. Standard laser systems typically provide pulses with durations ranging from a few hundred fs down to tens of fs, with full-width at half-maximum (FWHM) spectral widths of the order of a few tens of nm. For fs laser systems, achieving optimal contrast in imaging applications relies greatly on the quality of the laser pulse at the sample plane. Propagation through dispersive elements on the way to the sample, especially highly dispersive elements such as high numerical aperture (NA) microscope objectives, results in chirped and temporally stretched non-Fourier transform-limited (non-FT-limited) pulses with reduced peak power at the focus of the objective [7,8]. Traditional pulse characterization techniques, such as interferometric autocorrelation, have intrinsic ambiguities/errors that increase for shorter pulses [9]. Such measurements can easily give an underestimation of the temporal duration, in particular for few-cycle pulses in the presence of high-order dispersion, due to the reduced coherence produced by high-order terms [10]. Furthermore, an autocorrelation measurement forcibly involves a setup external to the microscope workings, where the fs laser beam must be split into two replicas, with one of the replicas temporally delayed using a precision translation stage, and finally recombined with interferometric precision into a collinear beam prior to traversing the microscope [11].

Imaging strategies revolve around tuning the central wavelength of the laser to coincide with the two-photon absorption maximum of the chromophore or chromophores on the sample or, alternatively, using several excitation wavelengths and compiling a sequence of images. Both these methods have intrinsic drawbacks. In the former not all chromophores are efficiently excited and in the latter individual cell constituents cannot be tracked simultaneously, rendering fast processes at the cellular level impossible to track, and the longer exposure during multiple scans can further lead to photo-toxicity and photo-induced damage. Efficient simultaneous excitation of multiple different chromophores is therefore a highly desired capability in the field of bioimaging, and several techniques have been implemented in view of this goal. Individual excitation bands have either been combined in setups employing multiple detectors [12–14] or measured sequentially with a single detector configuration [15]. Another strategy involves using sub-10-fs ultra-broadband fs lasers [16], where the emitted spectra can span up to several hundred nm, approaching the full effective gain bandwidth of the laser medium. The broad emission can excite multiple chromophores with distinct absorption spectra which have been shown to be separately detectable either by spectral analysis in mixed liquid samples [17] or by intensity measurements with multiple channel detectors on 2D samples [18]. Different parts of the ultra-broadband laser spectrum can also be used to access different imaging modalities simultaneously, such as combining coherent anti-Stokes Raman scattering (CARS) with two-photon fluorescence and second-harmonic generation (SHG) [19]. The important parameter space of fluorescence lifetime imaging microscopy (FLIM), a technique capable of differentiating between several dyes even when the signal originates from the same excitation volume [20,21], have not so far been explored with ultra-broadband excitation. FLIM is the technique behind multi-photon fluorescence lifetime imaging microscopy (MP-FLIM), a powerful tool in cell biology and bioimaging applications. Time-correlated single-photon counting (TCSPC) [22] is one way of implementing FLIM. Herein, each detected photon is given a time stamp in relation to the pulsed excitation, and a photon arrival time histogram is created, which can be related to the fluorescence decay time of the chromophores. The lifetime of the single chromophore depends on the local environment, where FLIM microscopy can deliver information about protein interaction, metabolic state and conformation changes [22].

Biomedical Optics EXPRESS

In this paper we present the SyncRGB method, which enables simultaneous tracking of multiple chromophores within a single scan and with a single detector. To show the merits of the SyncRGB method with an ultra-broadband 7 fs laser, a comparison with the standard method based on a relatively narrowband tunable 70 fs laser is performed. For the comparison, both intensity and, for the first time, TCSPC imaging are used as measuring modalities. In the experiments, both laser systems are coupled to a custom-built inverted multi-photon microscope equipped with a single detector and optimized at the focus either via standard autocorrelation measurements (narrowband laser) or by using the d-scan ultrashort pulse characterization technique (ultra-broadband laser).

2. Materials and methods

2.1 Sample preparation

For 2D images, a multicolor-labeled 2D FluoCells #1 (Thermofisher) test sample containing bovine pulmonary artery endothelial cells (BPAEC) with DAPI labeling the nuclei, Alexa Fluor 488 the actin filaments and MitoTracker Red labeling mitochondria was employed. Adapted two-photon absorption [23,24] spectra for DAPI, Alexa Fluor 488 and MitoTracker Red can be seen in Fig. 1(a).

For 3D imaging and large area 2D scans, swine carotid samples were used. All procedures for provision of animal samples were approved by the Direção Geral de Alimentação e Veterinária, Portugal (No. 15.078.UDER). Swine carotid arteries were supplied by a local slaughter house (Carnes Landeiro, S.A., Barcelos) and transported to the lab on ice. Upon arrival to the lab, arteries were rinsed with saline buffer (PBS - phosphate-buffered saline) and loose connective and fatty tissues were removed. The samples were stored in –80°C storage freezers. A 2-mm-tall tubular section of an artery was cut from the thawed sample and mounted standing on a #1.5 coverslip. Before the experiments, samples were thawed at room temperature for 30 minutes, then incubated with nuclei staining Hoechst 33342 solution (Life Technologies) diluted to 1 µg/mL in MilliQ water for 20 min to label the cell nuclei of the endothelial layer of the artery wall. The carotids were washed three times with PBS solution and embedded in a 7% gelatin solution (in PBS) for support and conservation.

Biomedical Optics EXPRESS

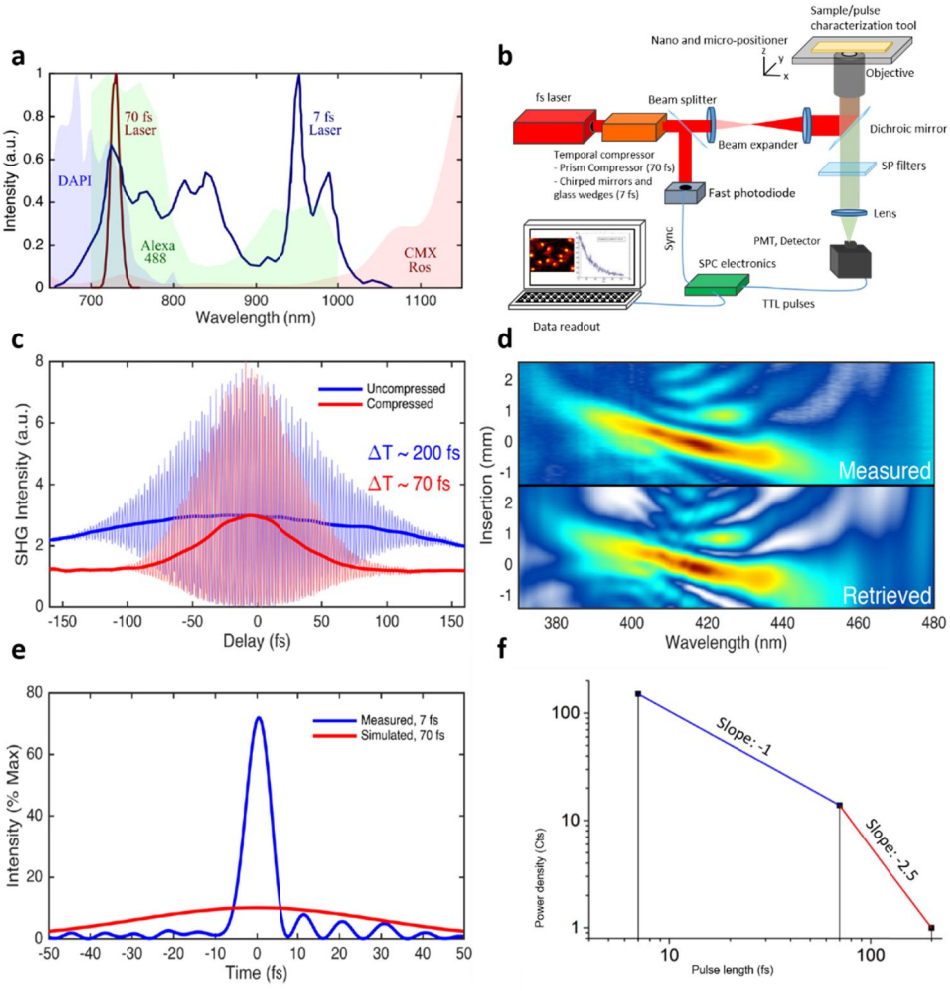

Fig. 1. SyncRGB conditions and setup. a) Laser sources and chromophores: a) Normalized spectra of the 70 fs and 7 fs laser systems and adapted single photon absorption spectra of dyes on the FluoCells #1 sample. b) Multi-photon fluorescence lifetime imaging microscopy (MP-FLIM) setup based on a femtosecond laser source, temporal compressor and a sample scanning inverted microscope setup equipped with a single PMT detector synchronized with the pulsed laser Sync signal via fast single-photon counting electronics. The measuring head of the d-scan pulse characterization and compression system is mounted at the sample position in the focus of the objective to determine and compensate the dispersion due to the used high-NA microscope objectives before performing MP-FLIM imaging experiments. c) Autocorrelation measurements of the narrow band fs laser in the uncompressed (blue, 200 fs) and compressed pulse configurations (red, 70 fs), measured on target. The Fourier-limited duration of the narrowband laser is 70 fs, hence the autocorrelation measurements indicated that the laser was close to optimum compression. d) d-scan measurements of the pulse on target. Top: measured d-scan trace. Bottom: retrieved d-scan trace, corresponding to a 7 fs pulse at optimum compression. e) Comparison of measured pulse shapes: Blue - 7 fs pulse measured on-target with d-scan, having almost 80% of the transform limited peak power. Red - Gaussian pulse with 70 fs intensity FWHM and the same energy as the blue curve. f) Pulse-length-dependent intensity signal strength of DAPI. Intensities are compared with spectral power density and overlap where two photon absorption of DAPI has been considered. Size of data points represents the uncertainty.

Biomedical Optics EXPRESS

2.2 Experimental setup

As a standard multi-photon excitation source we use a Ti:Sapphire laser oscillator (Tsunami 3969-15HP, tuning range 700-1080 nm, Spectra-Physics, Newport) with a repetition rate of 80 MHz pumped by a 15W 532 nm DPSS (diode-pumped solid-state) laser (Spectra-Physics Millennia 15). The oscillator is tuned to 775 nm or to 730 nm (as seen in Fig. 1(b)) and laser power is controlled by reflective ND filters. For compression and compensation of the group delay dispersion (GDD) of the complete microscope system (approximately 4000 fs^2) we used a prism compression setup composed of an SF10 prism, a corner cube and a rooftop mirror [25] through which the laser passes four times.

The ultra-broadband 7 fs laser system is a custom-built single-box Kerr-lens mode-locked laser oscillator (Enora, Sphere Ultrafast Photonics) with an output spectra practically covering the full tuning range of the Ti:Sapphire crystal (660-1065 nm, as seen in Fig. 1(b)). This octave-spanning laser system and its detailed temporal and spectral characterization have been described elsewhere [26,27]. Dispersion pre-compensation, pulse compression and measurement at the focus of the microscope objectives was performed with a d-scan system (Sphere Ultrafast Photonics).

The laser pulses are guided into a custom-built microscope (see Fig. 1(b)) based on an inverted microscope platform (R21, MadCityLabs) by steering silver mirrors, and expanded by a set of lenses. The sample scanner is a combined micro- and closed-loop nano-positioning system (NanoLPS200, MadCityLabs) controlled by a self-developed device control software (Labview). To reduce dispersion and wavefront distortions on the excitation path we use a thin-film metallic mirror (ND05B, Thorlabs). The metallic mirror has a transmission of 30% associated with a signal loss at the detector when compared to the multi-photon dichroic mirror (T680-SPRX, AHF F73-678) that we use for measurements with the uncompressed 200 fs laser system, with >90% transmission in the multi-photon signal range of 400-670 nm and >90% reflection over 700-1080 nm. In our comparison of the effect of pulse length on the signal strength this loss is adequately accounted for. Signal collection is done in EPI/reflection mode via the microscope objective, and to ensure detection of the multi-photon signal, a PMT (H7422P-40 Hamamatsu, 5 mm diameter active area, spectral sensitivity range 300-720 nm) is used for detection together with a transfer lens. For multi-photon imaging on 2D cell samples, a 1.3 NA oil-immersion objective (100 × , WD 0.17 mm, CFI Plan Fluor, Nikon) is used. A 0.75 NA dry objective (40 × , WD 0.66 mm, Plan Fluorite Nikon) is used for deep tissue scanning. The emission filters used were a short pass filter (FF01-680/SP-25 Blocking edge Brightline, Semrock), combined with a DAPI (FF02-447/60-25, Brightline, Semrock) and three Schott BG39 bandpass filters in series, if nothing else is indicated. The PMT module is read out by a single channel TCSPC module from Becker & Hickl, Berlin (SPC-130).

2.3 Pulse characterization at-focus of a high NA microscope objective

To characterize the narrowband pulse, we placed a pass-through interferometric autocorrelator in the beam path leading to the microscope, which creates a collinear beam with two pulse replicas of variable delay. This beam is then sent to the microscope and focused by the same objective that will be used for the imaging experiments. The effect of pulse compression of the narrowband laser system is seen in Fig. 1(c), where the obtained pulse widths are 200 fs for the uncompressed and 70 fs for the compressed pulse. In the case of the ultra-broadband laser we used a commercial d-scan compressor designed for high-NA objectives (Sphere Ultrafast Photonics) at the output of the 7 fs laser, before sending the beam to the microscope. In both cases the broadband SHG signal is detected with a commercial SHG measurement head designed for microscopes (Sphere Ultrafast Photonics). This measurement head is designed such that the second harmonic crystal can be precisely positioned at the focus of the objective, and the generated SHG signal is then detected with a fiber spectrometer. In the autocorrelation case the signal was spectrally integrated to yield the

Biomedical Optics EXPRESS

interferometric autocorrelation trace. In the d-scan case the insertion-dependent, frequency-resolved signal was analyzed using the d-scan algorithm, as seen in Fig. 1(d) for the broadband 7 fs laser system. The retrieved peak power for both laser systems based on the d-scan measured pulse shapes is shown Fig. 1(e).

3. Results and discussion

3.1 SyncRGB imaging

By adjusting the intracavity dispersion of the ultra-broadband 7 fs laser, its spectral profile can be optimized to match the absorption of various dyes in a multicolor labeled sample, as shown in Fig. 1(a), while maintaining a very broad bandwidth of more than 320 nm (measured at −10 dB in intensity) capable of supporting few-cycle pulse durations. Also the dispersion can be adjusted such that variations in the fluorescence quantum yield of the fluorescent labels can be accounted for by altering the relative weight of selected spectral components. Imaging is performed in a simple single detector microscope setup coupled to TCSPC electronics [22] (see Fig. 1(b)). Temporal pulse compression of both lasers is achieved directly at the focus of the microscope objective with the recently established d-scan technique [26,28]. Besides its in-line single-beam implementation and intrinsic few-cycle measurement capabilities, d-scan effectively provides the complete temporal profile of the pulses (intensity and phase) at the sample plane. Furthermore, the measured d-scan trace is a very intuitive tool for optimizing the spectral phase of the pulses and achieving maximum compression (see Fig. 1(c, d and e)).

Multi-photon images created with the uncompressed and compressed standard 70 fs oscillator and with the ultra-broadband 7 fs oscillator are given in Fig. 2. For the first comparative analysis, only the total intensity (i.e. the integral of the TCSPC decay trace intensity in each pixel) will be regarded, while in the second part the TCSPC decay curves are analyzed for the same data.

In the first part, three representative positions inside the cell nucleus (DAPI), cytoplasm (AlexaFlour488 and MitoTracker Red) and a cell-free area (background) were chosen in each image. Comparing the multi-photon image data shown in Fig. 2(a1, a2) and Fig. 2(b1,b2) reveals up to 12 times higher signal intensity for compressed (≈70 fs) as compared to uncompressed standard fs oscillator pulses (≈200 fs), which is a factor of 2 higher than reported in Ref [29]. The intensity gain corresponds to a $\tau^{-2.5}$ dependence on the pulse duration τ (see Fig. 1(d) in the Supporting Information). This increase is larger than the theoretically predicted τ^{-1} dependence [30,31], which clearly indicates the presence of higher-order phase terms, apart from the linear chirp, in the uncompressed 200 fs pulses.

Furthermore, the signal-to-noise ratio (S/N) in the case of DAPI improves considerably from S/N≈14 to S/N≈165 via pulse optimization. For cytoplasm areas we observe an increase from S/N≈2 to S/N≈19 upon at-focus pulse compression. Assignment of a common value for the cytoplasm areas stems from the single channel detection where intensity signals from both chromophores are detected simultaneously and not spectrally distinguished. Furthermore, for the excitation wavelengths provided by the standard laser system, only Alexa Fluor 488 will be efficiently excited in the cytoplasm, as seen in the spectral overlap in Fig. 1(a). The general enhanced sensitivity using the compressed pulses results in finer details being resolved in the multi-photon intensity image, here observed for higher DAPI signal contrasts within the nucleus in Fig. 2(b1) vs. 2(a1), and increased visibility of the actin filaments in Fig. 2(b2) compared to Fig. 2(a2).

Biomedical Optics EXPRESS

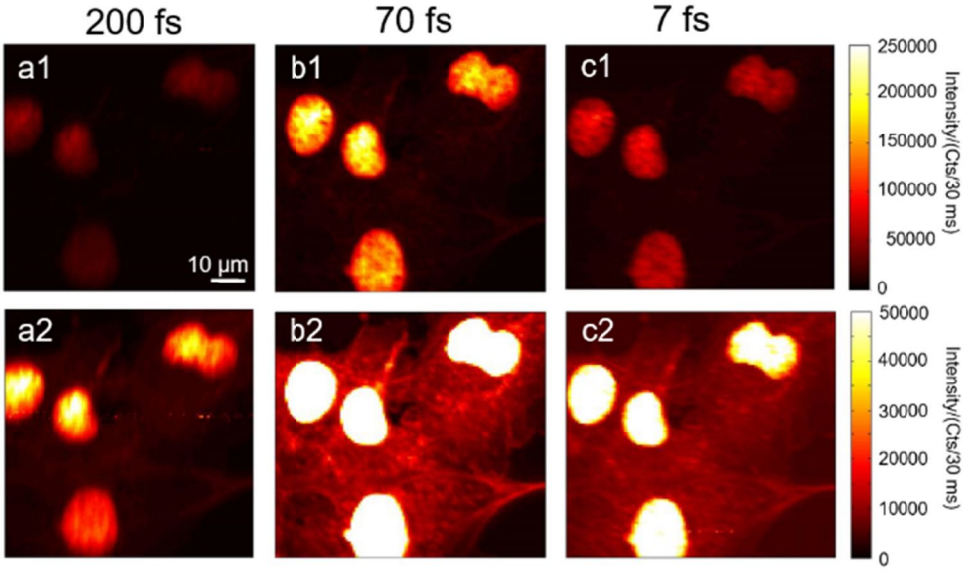

Fig. 2. Comparison of S/N in multi-photon images taken with different laser sources. Top row and bottom row show identical data using different color maps. (a1, a2) Uncompressed (200 fs) and (b1, b2) compressed (70 fs) pulses from the standard laser oscillator. (c1, c2) Compressed few-cycle 7 fs laser. Scale bar in a1 is 10 µm and is used for all images; all images are 110 × 110 pixels with a pixel dwell time of 30 ms = 363 s/scan.

Figures 2(c1,c2) show the intensity images taken at the identical area of the FluoCells sample using the few-cycle 7 fs laser system with the same average power as used for the 70 fs system (36 mW). The highest intensity is again found for the DAPI stained cell nuclei areas but the apparent signal intensity is lower compared to the image recorded with the 70 fs laser. The reason is the broadband nature of the 7 fs laser system, where approximately only 41% of the spectral power is absorbed by DAPI, as can be seen by the spectral overlap shown in Fig. 1(a). Including the spectral overlap in the intensity calculations for the DAPI signal, a relative increase of 10 times is observed, when the pulse duration is changing from 70 fs to 7 fs. The resulting intensity levels for the laser oscillators at 70 fs and 7 fs follow the predicted τ^{-1} dependence on pulse duration (see Fig. 1(f)). A deviation from the τ^{-1} behavior at short pulse durations as in Ref [31] is not observed, indicating that both systems are indeed near Fourier-transform-limited (FT-limited) at the sample position, where especially the large dispersion through the high NA objective has been adequately compensated for up to at least third-order.

In the experiments, the average laser power of 36 mW is relatively high but especially for the 7 fs laser is still below the threshold for derivation from the square dependency between excitation power and fluorescence yield [17]. The relatively long pixel dwelling time combined with the high peak power of the FT-limited pulses in our experiments induces no observable photo induced damage even for the few-cycle broadband laser [32,33]. It is not possible in these experiments with fixed cells to identify the possible additional photo toxicity or onset of hyper-fluorescence induced by the use of few-cycle broadband laser pulses [18].

For the few-cycle laser the measured S/N varies for the different cell positions and both intensity and background values have been extracted directly from the data and not corrected for spectral overlap. The highest value is observed for the cell nucleus (DAPI) (S/N≈27) and lower values for areas in the cytoplasm, which contain Alexa Fluor 488 and MitoTracker Red for which we assign a common S/N≈3. In contrast to the narrowband 70 fs laser system, the broadband 7 fs few-cycle laser can efficiently excite both chromophores in the cytoplasm, so the intensity signal originates from both chromophores. This can be shown by adding a

Biomedical Optics EXPRESS

RG630 bandpass filter in the detection path, efficiently blocking the BG (Blue-Green) components. Multi-photon images in Fig. 3 are recorded respectively with the narrowband 70 fs and the ultra-broadband 7 fs laser excitation sources without (Fig. 3(a) and 3(b) and with (Fig. 3(c) and 3(d)) the R (Red) bandpass filter.

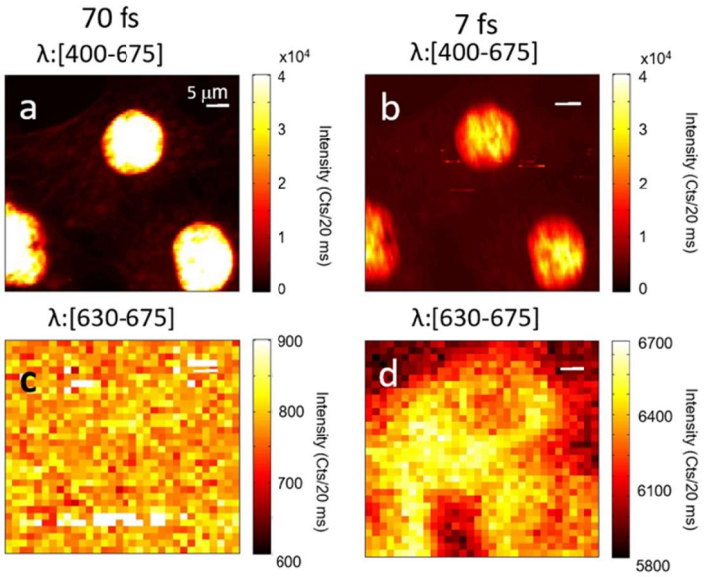

Fig. 3. SyncRGB imaging using a 7 fs source. Multi-photon intensity images of the same sample areas taken with the compressed 70 fs Ti:Sapphire laser (a, c) and with the broadband 7 fs laser source (b, d). For both lasers, two filter configurations were chosen, either a 685 nm short pass filter that transmits the emission wavelength ranges of all three chromophores (top), or in addition a RG630 filter was placed in front of the detector – selective for the Mitochondria label: MitoTracker Red (bottom). For the 70 fs laser no MitoTracker Red fluorescence is detected (c), whereas the 7 fs excitation pulses enable detecting intensity contributions inside the cell cytoplasm (d). Scale bar in (a) is 5 µm and is used for all images and a pixel dwell time of 20 ms for all images. (a-b) are 100 × 100 pixels = 200 s/scan while (c-d) are 32 × 32 pixels = 20.5 s/scan.

A direct comparison of the multi-photon images without the RG630 filter shows approximately twice as high apparent signal intensity for the DAPI-stained cell nuclei excited by the 70 fs system (a) as compared to the 7 fs laser system (b), similar to the findings in the last section. In the cytoplasm region of the cells the opposite effect is observed, showing an approximately 1.2 times higher intensity for the 7 fs system as compared to the 70 fs system, in good agreement with the spectral overlap of the broadband 7 fs laser system with all three chromophores where the 70 fs system is only resonant with DAPI and Alexa Fluor 488. With the RG630 filter inserted, a featureless background signal without any fluorescence signal is observed for the 70 fs laser (Fig. 3(c)), indicating no excitation of MitoTracker Red, while fluorescence signal originating from the cytoplasm regions of the cell is observed under the same conditions for the few-cycle 7 fs laser (Fig. 3(d)).

In the current system a major limiting factor, as seen from the intensity data, is the S/N-ratio for the few-cycle 7 fs laser system. The background level is nearly twice as large compared to both the compressed and the uncompressed standard fs oscillator. The additional background contribution stems from the short wavelength tail of the broadband laser spectrum which overlaps with part of the fluorescence emission spectra and is therefore not completely cut by the used standard multi-photon emission and bandpass filters. Apparent signal strength is also lower as a consequence of the broad spectrum with a lower spectral power available to efficiently excite each chromophore. The 7 fs laser will on the other hand

Biomedical Optics EXPRESS

give rise to additional nonlinear signal strength caused by both degenerate and non-degenerate mixing of its spectral components, which is not addressable with the narrowband laser [17].

3.2 SyncRGB - selectivity based on FLIM

In the second part of the analysis we take full advantage of the recorded TCSPC measurement data. Each photon detection event is associated to one of 1024 bin channels equally dividing the 12.5 ns long repetition rate intervals of the 80 MHz femtosecond laser pulses, whereby an arrival time histogram and subsequently a decay curve is created. While the histograms recorded in the nuclei regions are close to the saturation level which may lead to a maximum 5%-10% overall deviation of fluorescence lifetime values determined in this region [34], areas in the cytoplasm regions are optimized for FLIM analysis. The fit of the decay curves in each pixel is based on a method described in [35]. The algorithm allows a varying number of exponential decays contributing to the multi-exponential fit. This allows each pixel in the image to be fitted with the best possible linear combination. While the algorithm allows extracting all contributing lifetime components with their weights, here we choose to present the resulting average fluorescence lifetime in the form of FLIM images (Fig. 4) that relate to the intensity images shown in Figs. 2(b1,b2) and 2(c1,c2), respectively. We use the same lifetime color bar for both images. In the experiments the instrument response function (IRF) was determined from signal analysis from a reflective sample for both laser systems.

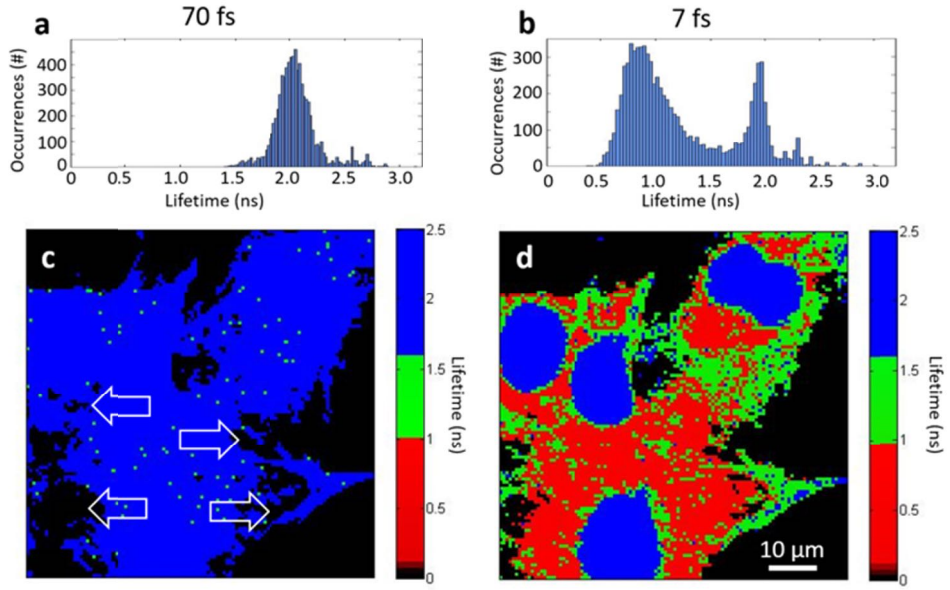

Fig. 4. SyncRGB FLIM using ultra-broadband laser excitation for MP-FLIM. MP FLIM images of 2D FluoCells #1 sample. Average fluorescence lifetime histogram for the a) 70 fs and b) 7 fs laser systems. c) 70 fs system at 730 nm, showing only resonant absorption with DAPI in the cell nuclei and Alexa Fluor 488 in the cytoplasm giving rise to one lifetime throughout the cell. White arrows indicating areas without fluorescence intensity in the case of the 70 fs laser system. d) 7 fs few-cycle laser system resonant with all three chromophores on the sample, giving rise to three distinct lifetimes throughout the cell and enabling identification of distinctive cell constituents. Especially the areas indicated by the white arrows for the 70 fs system are actively fluorescing for the 7 fs. All images are 110 × 110 pixels with a pixel dwell time of 30 ms = 363 s/scan.

As seen in in Fig. 4(a, b) the average fluorescence lifetime histogram distributions of the same sample area recorded with the two laser systems are very different from each other. For the 70 fs laser a single broad peak centered at 2 ns is observed containing signal contributions

Biomedical Optics EXPRESS

from DAPI and Alexa488 dyes. The 7 fs laser allows effective excitation of all three labeling dyes and a more complex structured histogram is observed. Interestingly, average fluorescence lifetime contrast can be established for all RGB dyes (Fig. 4(d)); the weighted average fluorescence lifetime ranges suited to distinguish the main contributing dye per pixel are [1.8 - 2.5 ns], [1 - 1.5 ns] and [0.2 – 1 ns], for DAPI, Alexa488 and MitoTracker Red dominance, respectively. Applying the same ranges for the 70 fs laser, no contrast is observed in the image between the DAPI stained nuclei and the Alexa488 in the cytoplasm. Some image areas appear without signal (indicated by arrows in Fig. 4(c)); these are pixels where only MitoTracker Red is present and therefore no signal contribution occurs for the non-resonant 70 fs laser system. This argumentation is further supported by the observed differences of the average fluorescence lifetime values in the cytoplasm. In case of the 7 fs laser, in large areas of the cytoplasm a mixing of the Alexa488 signal with the very short fluorescence lifetime MitoTracker Red emission may lead to an overall shortened average fluorescence lifetime. Thus, compared with the 70 fs image, where Actin areas appear with 1.6 and 2.8 ns, in the case of the 7 fs laser the average value is lower at 1.3 +/– 0.3 ns. The resulting contrast in lifetime presents a convenient method for distinguishing different biologically relevant components within a cell.

3.3 SyncRGB application on a bio-tissue sample

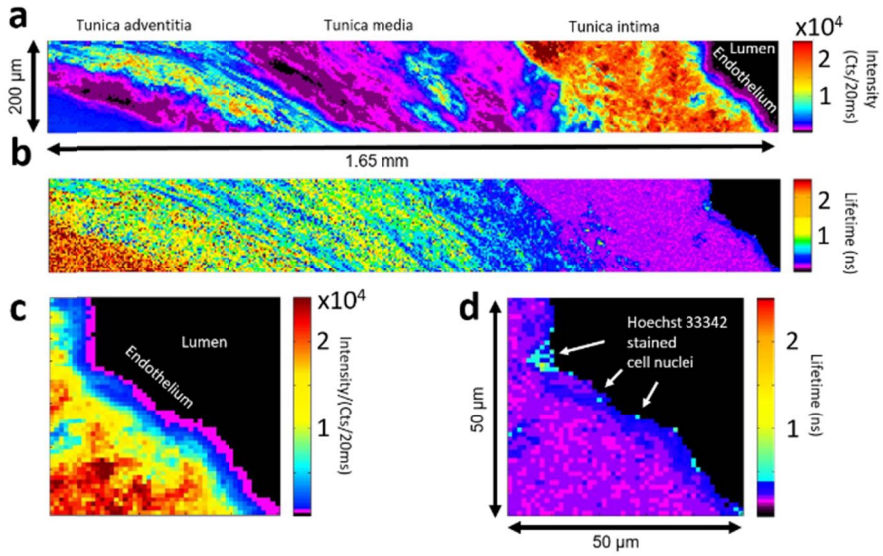

Fig. 5. Large area SyncRGB intensity and lifetime imaging on a pig artery sample with Hoechst 33342 stained cell nuclei. a) Large area fluorescence intensity image of a pig artery. The image is stitched together from 11 individual 200 × 200 µm (50x50 pixels) scans with 50 µm overlap and a pixel dwell time of 20 ms = 50 s/scan. Major elements of the artery are indicated and can be distinguished by their fluorescence signal contribution. b) SyncRGB image of the large scan area using MP-FLIM. c) Close up intensity image of the endothelium part where the weak fluorescence and concentration of the Hoechst 33342 stained cell nuclei make them not clearly identifiable against the autofluorescent background. d) Close up image of the endothelium part clearly showing the position of Hoechst 33342 stained cell nuclei. The positions of Hoechst 33342 stained cell nuclei are indicated by arrows.

Further application of the SyncRGB technique using the 7 fs laser system on a non-standard biological sample is shown in Fig. 5(a), which shows a large area cross section intensity image of the pig artery sample stitched of individual multi-photon 200 × 200 µm fluorescence images scanned with the few-cycle 7 fs laser system. Major artery elements, Tunica adventitia, Tunica media and Tunica intima are indicated above the image and are also

Biomedical Optics EXPRESS

representative for Fig. 5(b), which shows the corresponding MP-FLIM image; corresponding wide-field transmission mode images of a similar sample are shown in Fig. S4 in the Supporting Information. In the stitched images the lumen of the artery is seen on the far right and the first fluorescence layer is the thin endothelium where the cell nuclei are stained with Hoechst 33342 and the layer is 20 to 40 µm wide.

In Fig. 5(a) and especially in the zoom of the lumen region in Fig. 5(c) the individual stained cell nucleus cannot be identified in the endothelium layer but the relatively low concentration of cell nuclei and the short extension of the layer give rise to an overall weak fluorescence signal. The high concentration of various types of collagen and elastin in the adjacent layer produces a very strong auto fluorescence/SHG signal upon excitation and is referred to the Tunica intima reaching about 0.5 mm into the artery wall. The packing of collagen and elastin is gradually thinning out with increasing distance from the lumen whereby the auto fluorescence signal decreases with heterogeneous autofluorescence levels in Tunica media and Tunica adventitia. The large area MP-FLIM shows fluorescence lifetime differences between the Tunica layers; for the high content collagen elastin layer a short fluorescence lifetime is observed (< 0.2 ns), while medium and final Tunica reach about 0.5 ns and >1 ns, respectively. In the zoomed MP-FLIM image of the epithelial layer, the nuclei become observable by their fluorescence lifetime contrast and associated locations.

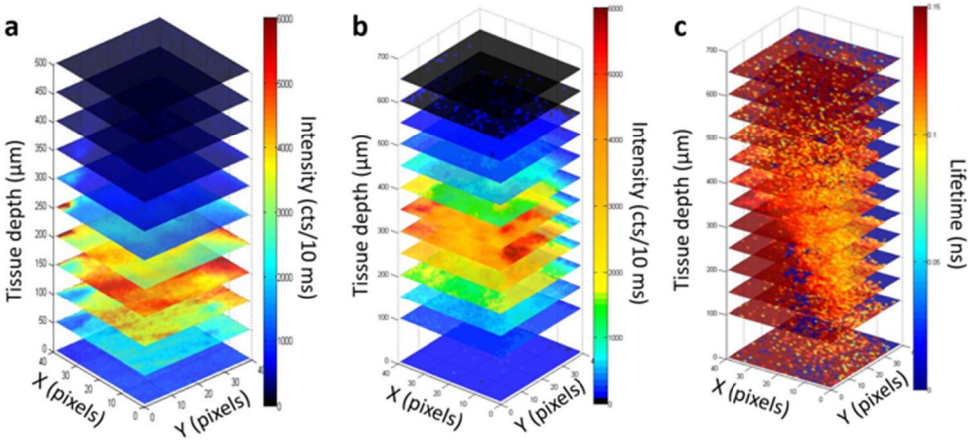

Fig. 6. Pulse-regime-dependent deep tissue scanning on a pig artery stained with Hoechst 33342. a) 70 fs laser based deep tissue multi-photon image stack. b) 7 fs laser based multi-photon image stack. c) SyncRGB MP-FLIM deep tissue stack using the 7 fs laser. Individual scans are 200 × 200 µm with 40 × 40 pixels and pixel dwell time of 10 ms = 16 s/scan. Besides increased depth sensitivity observed for the ultra-short laser, the FLIM detection enables identifying similar composition tissue areas.

In Fig. 6 the pulse-regime-dependent deep tissue scanning ability of the method is shown. Scanning with a 40 × microscope objective gives a large field of view (FOV) but the relative low NA of 0.75 will limit collection efficiency compared to specialized high-NA multi-photon physiology objectives. For our scans we define z = 0 just outside the sample, where the detection signal falls to the background, and thus the first image of the scan is featureless, additional scans were performed every 50 µm in z-direction. Laser power was attenuated to 32 mW for the 7 fs laser and 37 mW for the 70 fs laser and the pulses were compressed at the focus.

In our experiment we do not compensate for additional phase distortion and chirping of the laser pulse when entering the scattering tissue and we have not compensated the power loss associated to deep tissue scanning. Optimization of both quantities should give rise to additional signal strength and penetration depth [36]. The low laser power used for the scans

Biomedical Optics EXPRESS

gives a negligible contribution from out-of-focus chromophores to our measured intensity signal. Scans for both laser systems are optimized to the same intensity level and the background level is set higher for the 7 fs laser system compared to the 70 fs system.

Comparing Fig. 6(a) and 6(b) we see that we are able to retrieve a fluorescence signal for the 7 fs laser system from a depth of at least 600 µm, close to the working distance (WD) limit of the objective as compared to around 400 µm for the 70 fs laser system, which is in agreement with results in Refs [31,37–39]. – i.e., shorter pulse durations have a higher depth limit. Both laser systems show an increased collection efficiency for scan depths deeper than the sample surface, where the additional intensity contribution stems from a collection of scattered two-photon fluorescence photons. The enhancement maxima for both laser systems are at scan depth positions approximately equal to the effective FOV, indicating a larger collection efficiency for the broadband few-cycle 7 fs laser. Figure 6(c) is the MP-FLIM image stack of Fig. 6(b) obtained with the SyncRGB method – ultra-broadband excitation and broadband detection using a single detector attached to a TCSPC system, where the FLIM contrast helps identifying similar composition tissue areas.

4. Conclusions

In this work we demonstrate, for the first time, simultaneous excitation of multi-color labeled samples with chromophores in the red, green and blue (RGB) spectral range, which we accomplish by the use of an ultra-broadband few-cycle 7 fs laser source. Their signal can be detected e.g. via photon counting and wavelength filtering. We demonstrate that by using MP-FLIM detection and multi-exponential fitting of the photon arrival histograms, one can discern, in a single scan and using a single detector, nuclei, mitochondria, and F-actin, each labeled by different RGB chromophores. The ultra-broadband source effectively eliminates the need of laser wavelength tuning or multiple light sources resulting in potential faster scan times and reduced photo-induced damage. In this work we also show the advantage of shorter pulse length for achieving larger penetration depth in tissue MP imaging, reaching up to 50% deeper inside the tissue with the shorter 7 fs laser compared to the longer 70 fs laser.

Funding

CCDR-N via the project Nanotechnology-based functional solutions (NORTE-01-0145-FEDER-000019); Fundação para a Ciência e a Tecnologia (FCT), Portugal (grants ‘UltraGraf’ M-ERA-NET2/0002/2016, UID/ NAN/50024/2013); Network of Extreme Conditions Laboratories - NECL and CCDR-N (NORTE-07-0124-FEDER-000070, NORTE-01- 0145-FEDER-022096); PT2020 (program 04/SI/2016 - QI PME, grant no. 020751).

Disclosures

The authors declare that there are no conflicts of interest related to this article.

References

1. E. M. Phizicky and S. Fields, “Protein-Protein Interactions: Methods for Detection and Analysis,” Microbiol. Rev. **59**(1), 94–123 (1995).
2. S. W. Hell, “Far-field optical nanoscopy,” Science **316**(5828), 1153–1158 (2007).
3. M. Orrit, “Nobel Prize in Chemistry: Celebrating optical nanoscopy,” Nat. Photonics **8**(12), 887–888 (2014).
4. K. König, “Clinical multiphoton tomography,” J. Biophotonics **1**(1), 13–23 (2008).
5. X. Yang, H. Xie, E. Alonas, Y. Liu, X. Chen, P. J. Santangelo, Q. Ren, P. Xi, and D. Jin, “Mirror-enhanced super-resolution microscopy,” Light Sci. Appl. **5**(6), e16134 (2016).
6. W. Denk, J. H. Strickler, and W. W. Webb, “Two-photon laser scanning fluorescence microscopy,” Science **248**(4951), 73–76 (1990).
7. U. Fuchs, U. Zeitner, and A. Tünnermann, “Ultra-short pulse propagation in complex optical systems,” Opt. Express **13**(10), 3852–3861 (2005).
8. N. Accanto, J. B. Nieder, L. Piatkowski, M. Castro-Lopez, F. Pastorelli, D. Brinks, and N. F. van Hulst, “Phase control of femtosecond pulses on the nanoscale using second harmonic nanoparticles,” Light Sci. Appl. **3**(1), e143 (2014).
9. J. H. Chung and A. M. Weiner, “Ambiguity of ultrashort pulse shapes retrieved from the intensity

Biomedical Optics EXPRESS

autocorrelation and the power spectrum," IEEE J. Sel. Top. Quantum Electron. **7**(4), 656–666 (2001).
10. R. Trebino, *Frequency-Resolved Optical Gating: The Measurement of Ultrashort Laser Pulses* (Springer US, 2000).
11. J. Squier and M. Müller, "High resolution nonlinear microscopy: A review of sources and methods for achieving optimal imaging," Rev. Sci. Instrum. **72**(7), 2855–2867 (2001).
12. D. Entenberg, J. Wyckoff, B. Gligorijevic, E. T. Roussos, V. V. Verkhusha, J. W. Pollard, and J. Condeelis, "Setup and use of a two-laser multiphoton microscope for multichannel intravital fluorescence imaging," Nat. Protoc. **6**(10), 1500–1520 (2011).
13. P. Mahou, M. Zimmerley, K. Loulier, K. S. Matho, G. Labroille, X. Morin, W. Supatto, J. Livet, D. Débarre, and E. Beaurepaire, "Multicolor two-photon tissue imaging by wavelength mixing," Nat. Methods **9**(8), 815–818 (2012).
14. K. Wang, T.-M. Liu, J. Wu, N. G. Horton, C. P. Lin, and C. Xu, "Three-color femtosecond source for simultaneous excitation of three fluorescent proteins in two-photon fluorescence microscopy," Biomed. Opt. Express **3**(9), 1972–1977 (2012).
15. K.-C. Li, L. L. H. Huang, J.-H. Liang, and M.-C. Chan, "Simple approach to three-color two-photon microscopy by a fiber-optic wavelength convertor," Biomed. Opt. Express **7**(11), 4803–4815 (2016).
16. H. Studier, H. G. Breunig, and K. König, "Comparison of broadband and ultrabroadband pulses at MHz and GHz pulse-repetition rates for nonlinear femtosecond-laser scanning microscopy," J. Biophotonics **4**(1-2), 84–91 (2011).
17. C. Wang and A. T. Yeh, "Two-photon excited fluorescence enhancement with broadband versus tunable femtosecond laser pulse excitation," J. Biomed. Opt. **17**(2), 025003 (2012).
18. A. Klinger, L. Krapf, R. Orzekowsky-Schroeder, N. Koop, A. Vogel, and G. Hüttmann, "Intravital autofluorescence 2-photon microscopy of murine intestinal mucosa with ultra-broadband femtosecond laser pulse excitation: image quality, photodamage, and inflammation," J. Biomed. Opt. **20**(11), 116001 (2015).
19. I. Pope, W. Langbein, P. Watson, and P. Borri, "Simultaneous hyperspectral differential-CARS, TPF and SHG microscopy with a single 5 fs Ti:Sa laser," Opt. Express **21**(6), 7096–7106 (2013).
20. C. W. Chang, D. Sud, M. A. Mycek, and C. B. Mycek, "Fluorescence Lifetime Imaging Microscopy," Methods Cell Biol. **81**, 495–524 (2007).
21. T. Niehörster, A. Löschberger, I. Gregor, B. Krämer, H.-J. Rahn, M. Patting, F. Koberling, J. Enderlein, and M. Sauer, "Multi-target spectrally resolved fluorescence lifetime imaging microscopy," Nat. Methods **13**(3), 257–262 (2016).
22. W. Becker, A. Bergmann, E. Haustein, Z. Petrasek, P. Schwille, C. Biskup, L. Kelbauskas, K. Benndorf, N. Klöcker, T. Anhut, I. Riemann, and K. König, "Fluorescence lifetime images and correlation spectra obtained by multidimensional time-correlated single photon counting," Microsc. Res. Tech. **69**(3), 186–195 (2006).
23. F. Bestvater, E. Spiess, G. Stobrawa, M. Hacker, T. Feurer, T. Porwol, U. Berchner-Pfannschmidt, C. Wotzlaw, and H. Acker, "Two-photon fluorescence absorption and emission spectra of dyes relevant for cell imaging," J. Microsc. **208**(Pt 2), 108–115 (2002).
24. T. S. Viewer, "SpectraViewer," .
25. S. Akturk, X. Gu, M. Kimmel, and R. Trebino, "Extremely simple single-prism ultrashort- pulse compressor," Opt. Express **14**(21), 10101–10108 (2006).
26. M. Miranda, C. L. Arnold, T. Fordell, F. Silva, B. Alonso, R. Weigand, A. L'Huillier, and H. Crespo, "Characterization of broadband few-cycle laser pulses with the d-scan technique," Opt. Express **20**(17), 18732–18743 (2012).
27. R. Weigand, M. Miranda, and H. Crespo, "Oscilador láser de Titanio:zafiro de 2 ciclos ópticos Titanium:sapphire laser oscillator delivering two-optical-cycle pulses," in *Opt. Pura Apl.* (2013), p. 46(2), 105–110.
28. M. Miranda, T. Fordell, C. Arnold, A. L'Huillier, and H. Crespo, "Simultaneous compression and characterization of ultrashort laser pulses using chirped mirrors and glass wedges," Opt. Express **20**(1), 688–697 (2012).
29. G. McConnell and E. Riis, "Two-photon laser scanning fluorescence microscopy using photonic crystal fiber," J. Biomed. Opt. **9**(5), 922–927 (2004).
30. C. Xu and W. W. Webb, "Measurement of two-photon excitation cross sections of molecular fluorophores with data from 690 to 1050 nm," J. Opt. Soc. Am. B **13**(3), 481 (1996).
31. S. Tang, T. B. Krasieva, Z. Chen, G. Tempea, and B. J. Tromberg, "Effect of pulse duration on two-photon excited fluorescence and second harmonic generation in nonlinear optical microscopy," J. Biomed. Opt. **11**(2), 020501 (2006).
32. S. N. Arkhipov, I. Saytashev, and M. Dantus, "Intravital Imaging Study on Photodamage Produced by Femtosecond Near-infrared Laser Pulses In Vivo," Photochem. Photobiol. **92**(2), 308–313 (2016).
33. K. König, T. W. Becker, P. Fischer, I. Riemann, and K.-J. Halbhuber, "Pulse-length dependence of cellular response to intense near-infrared laser pulses in multiphoton microscopes," Opt. Lett. **24**(2), 113–115 (1999).
34. W. Be, "*The bh TCSPC Handbook 5th edition*," 891 (Springer, 2017).
35. J. Enderlein and R. Erdmann, "Fast fitting of multi-exponential decay curves," Opt. Commun. **134**(1–6), 371–378 (1997).
36. J. M. Dela Cruz, I. Pastirk, M. Comstock, V. V Lozovoy, and M. Dantus, "Use of coherent control methods through scattering biological tissue to achieve functional imaging," Proc. Natl. Acad. Sci. USA. **101**(49), 16996

Biomedical Optics EXPRESS

(2004).
37. P. Theer and W. Denk, "On the fundamental imaging-depth limit in two-photon microscopy," J. Opt. Soc. Am. A **23**(12), 3139–3149 (2006).
38. F. Helmchen and W. Denk, "Deep tissue two-photon microscopy," Nat. Methods **2**(12), 932–940 (2005).
39. E. Beaurepaire and J. Mertz, "Epifluorescence collection in two-photon microscopy," Appl. Opt. **41**(25), 5376–5382 (2002).